Supporting Information

Materials and methods

a. Fabrication of nanowire metamaterials. The nanowire metamaterials were fabricated by growing silver into the arrays of nanochannels in the anodic aluminium oxide (AAO) templates. Initially, a high-purity aluminum foil was polished in a mixed solution of 50% $HClO_4$ and C_2H_5OH (1:5 v/v) at 5°C under constant stirring. The finely polished aluminum foil was then patterned with hexagonal close-packed arrays of nano-identations using a focused 50 kV Ga-ion beam. The patterned foil was anodized in 0.3 M oxalic acid solution at the constant voltage of 40 V at 3°C. The nano-identations determine the position of the nanopores formed during the anodization, resulting in the nanochannel arrays with well defined lattice spacing (~100 nm) and an extremely narrow pore-size distribution. After the removal of the underlying remaining aluminium by a mixture of $CuCl_2$ and HCl, the oxide barrier at the base of the nanochannels was dissolved in a diluted H_3PO_4 solution. Subsequently, a layer of gold (400 nm) was deposited onto the bottom side of a free-standing AAO membrane using a UHV RF-Sputter machine in order to facilitate electric conductivity for electrochemical deposition of silver into the nanochannels. The electrolyte used for a DC electrochemical deposition was a mixture of KSCN and Ag_2SO_4. The final step of the process was a chemical mechanical polishing of the structure's top surface to ensure its flatness. In this way, a long-range hexagonally-ordered array of nanowires was obtained (Figure S1).
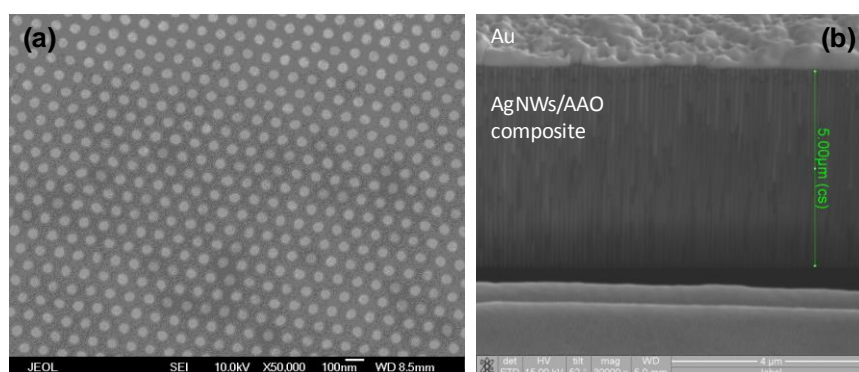
Figure S1. (a) Top-view and (b) cross-sectional SEM images of the nanowire metamaterial.

b. Dark-field spectroscopy. The optical properties of metamaterials were studied using far-field spectroscopy. The sample was illuminated by unpolarized white light from a halogen lamp in an inverted optical microscope working in the dark-field mode. In this way, oblique illumination was achieved and the back-scattered light was collected along the normal to sample surface. A 30 cm monochromator coupled to the liquid-nitrogen cooled charge-coupled device was used for spectral analysis.

c. Finite-element simulations. The optical properties of the metamaterials were modelled using full-vectorial finite-element simulations (COMSOL Multiphysics, RF Module). To model the nanowire arrays with a hexagonal close-packed lattice, the rectangular unit cell was adopted and periodic boundary conditions (Floquet periodicity) were applied in x- and y-directions (Figure S2). The optical constants of Ag are interpolated from Ref. S1 and the refractive index of AAO is $n_{AAO} = 1.6$.
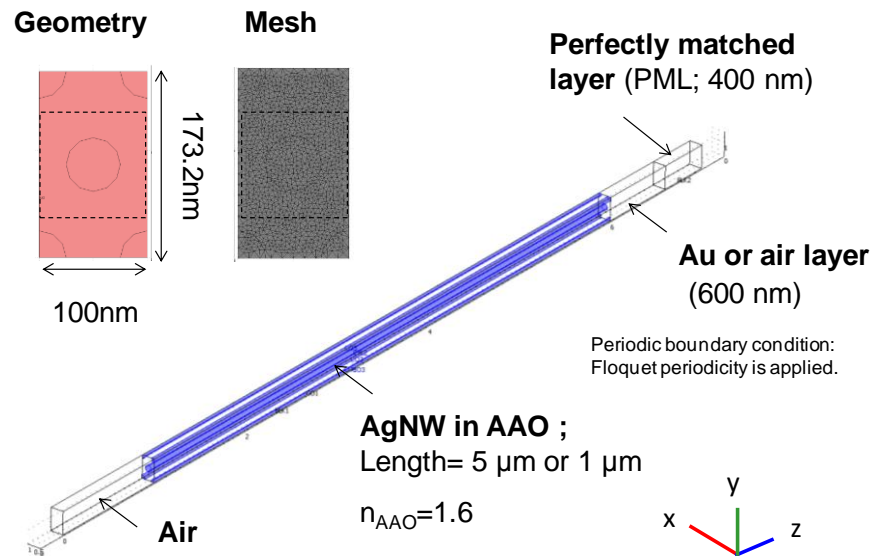
Figure S2. The geometry of the unit cell and the parameters used in the finite-element simulations of the hexagonal nanowire arrays.

d. Scattering-type scanning near-field optical microscopy. A scattering-type scanning near-field optical microscope[S2] (s-SNOM) was employed to map the near-field distributions of the electromagnetic field interacting with the metamaterial (Figure S3). The near-field was measured, in turn, at two wavelengths of 532 nm and 632.8 nm under a TM-polarized illumination at the 60° incidence angle. Under such illumination conditions, a tip apex acts as a vertically oriented nano-antenna and senses primarily the z-component of the local electric field. In order to minimise unwanted near-field interaction between the tip apex and the sample, a Pt-Ir-coated Si tip was used with the plasmonic resonance away from the excitation wavelengths. In order to separate a near-field contribution from a global scattering background, a dithering tip was employed, and the signal was detected at the 4th-harmonic of the tip oscillations. A heterodyne detection using a reference beam with a shifted frequency was used to measure both amplitude and phase of the near-field scattered radiation.[S3]
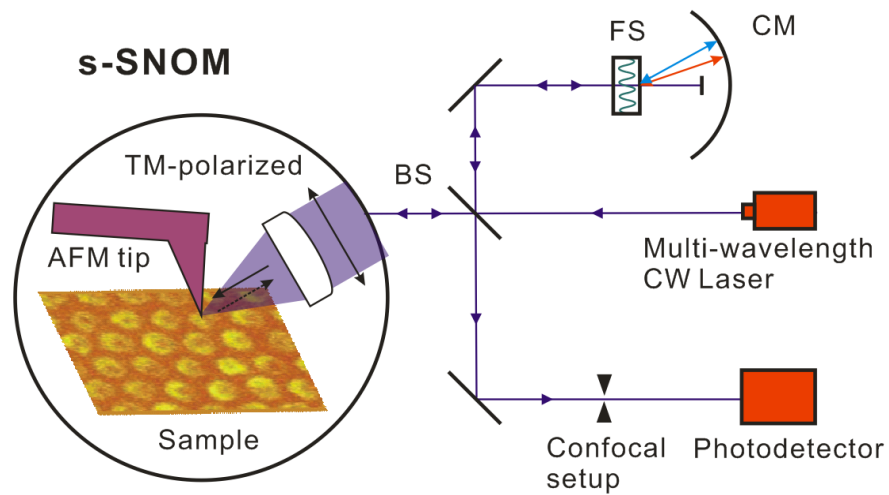
Figure S3. Schematics of a scattering-type scanning near-field optical microscope. CM: curved mirror; BS: broadband beamsplitter; FS: frequency shifter.

References for Materials and methods

S1.   Palik, E. D. Handbook of Optical Constants of Solids; Academic Press: New York, 1997.

S2.   Chu, J.-Y.; Wang, T.-J.; Chang, Y.-C.; Lin, M.-W.; Yeh, J.-T.; Wang, J.-K. *Ultramicroscopy* **2008,** 108, 314-319.

S3.   Keilmann, F.; Hillenbrand, R. *Phil. Trans. R. Soc. A* **2004,** 362, 787-805.

Supplementary Figures
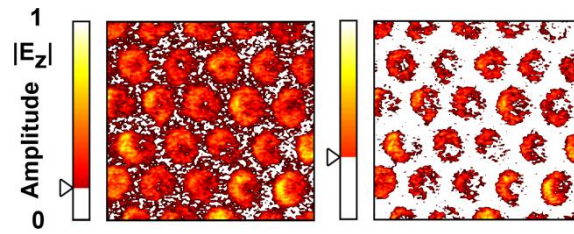
Figure S4. The near-field distributions as in Figure 2a with a contrast saturated at different levels as indicated by a marker.
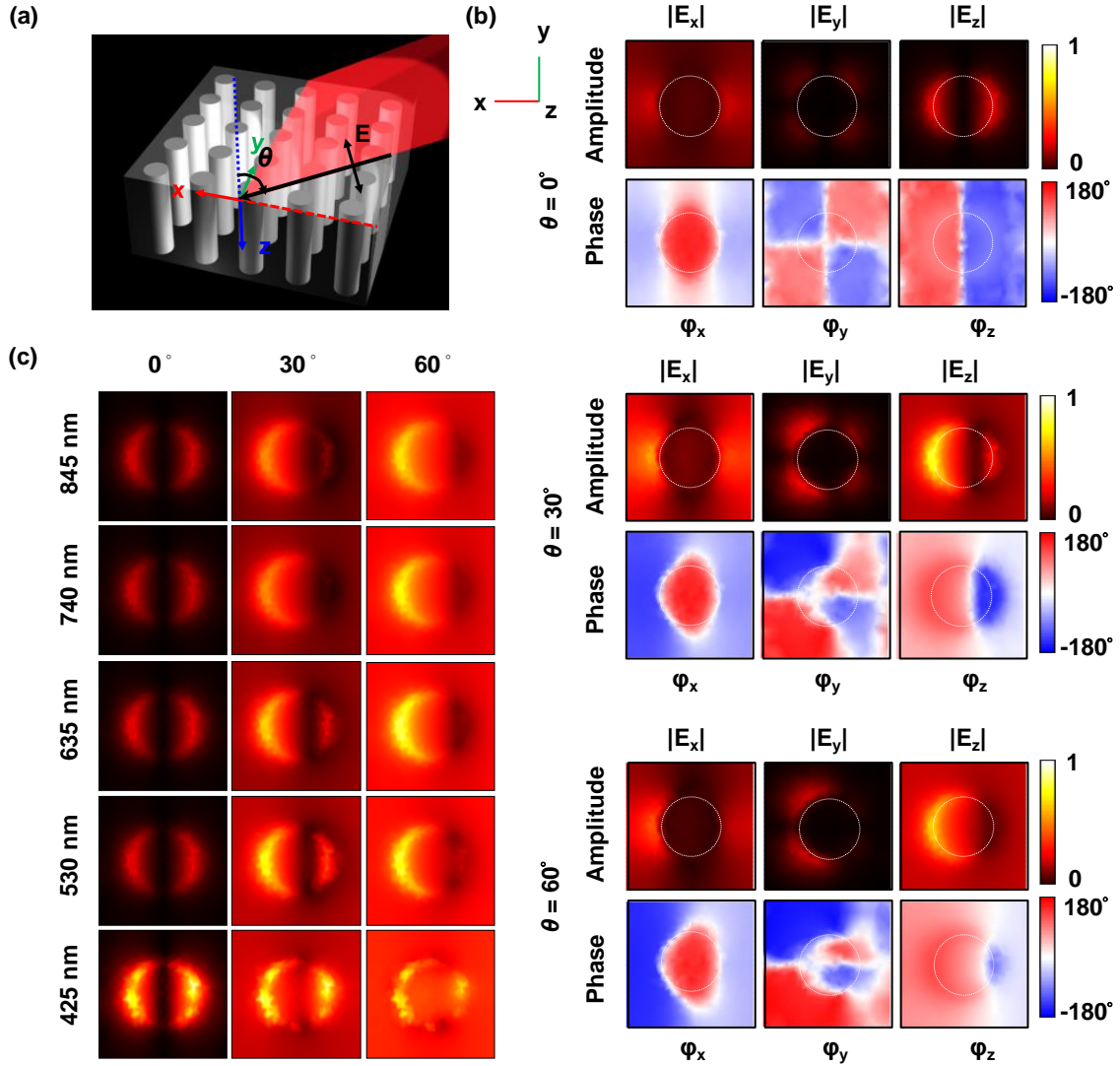
Figure S5. (a) Schematic of the nanowire metamaterial and the coordinate system in simulations. (b) Simulated amplitude and phase distributions of different field components at the angles of incidence θ = 0°, 30°, and 60°. The TM-polarised excitation light wavelength is 635 nm. (c) Simulated near-field |E$_z$| distributions for different wavelengths and angles of incidence. The distributions are calculated at the height of 5 nm above the nanowire metamaterial's surface. The metamaterial parameters are as in Figure 2. White dash lines outline the position of a nanowire.
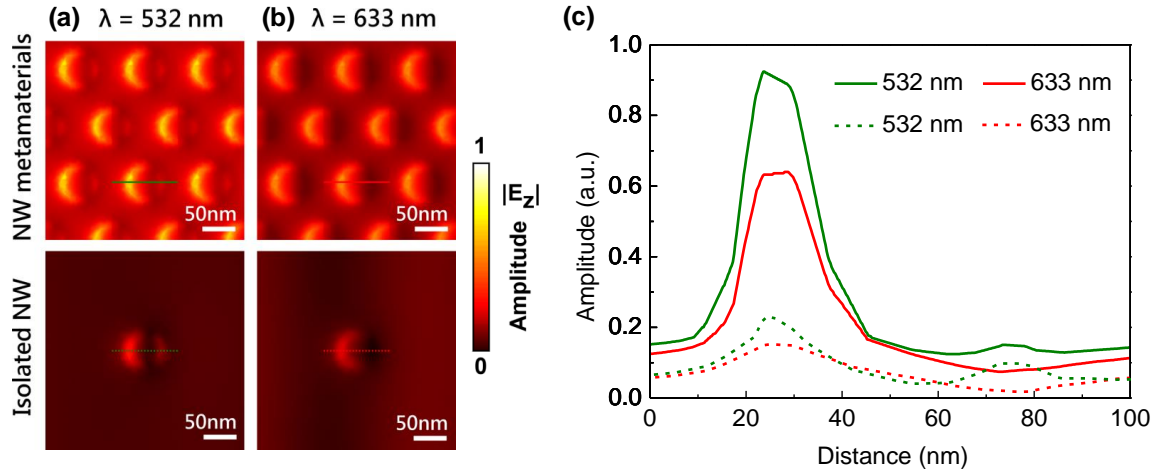
Figure S6. Simulated near-field $|E_z|$ distributions above the nanowire metamaterial and the isolated nanowire at the wavelengths of (a) 532 nm and (b) 633 nm, and (c) their cross-sectional plots (solid and dashed lines correspond to the metamaterial and the isolated nanowire, respectively). The distributions are calculated at the height of 5 nm above the nanowires' surface. The positions of the cross-sections are indicated by lines in (a) and (b). The metamaterial parameters are as in Figure 2.
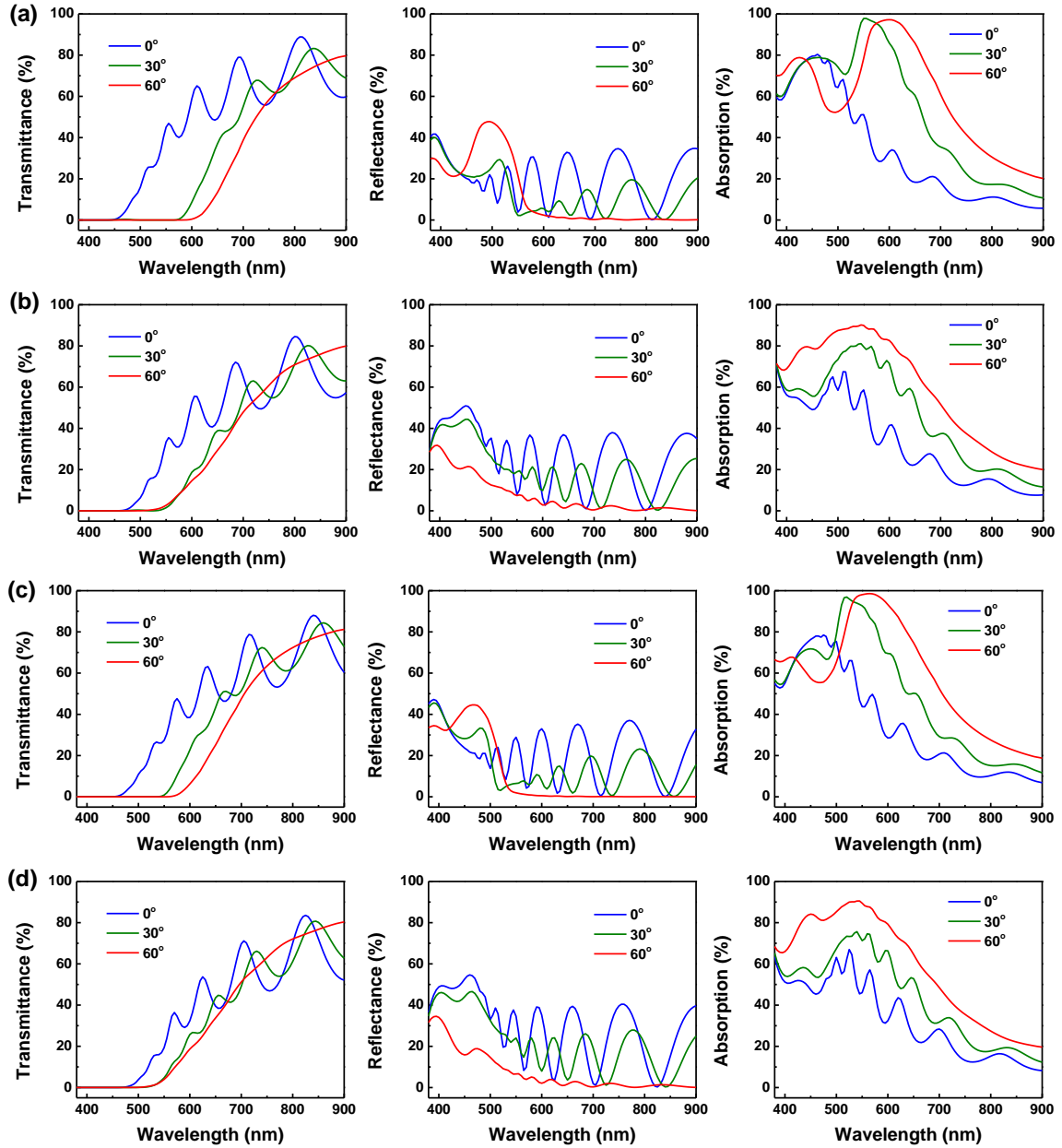
Figure S7. Simulated transmission, reflection and absorption spectra of the metamaterial at different angles of incidence obtained using (a,c) the effective medium approximation and (b,d) the nanowire/AAO composite for (a,b) square and (c,d) hexagonal close-packed lattices. All other metamaterial parameters are as in Figure 2.